

The importance of super-Eddington black hole accretion for the emergence of massive quiescent galaxies at high redshift

Evgenii Chaikin,¹ ¹ Joop Schaye,¹ Filip Huško,¹ Cedric G. Lacey,² Sylvia Ploeckinger,³ and Matthieu Schaller^{4,1}

¹Leiden Observatory, Leiden University, PO Box 9513, 2300 RA Leiden, the Netherlands

²Institute for Computational Cosmology, Department of Physics, University of Durham, South Road, Durham, DH1 3LE, UK

³Department of Astrophysics, University of Vienna, Türkenschanzstrasse 17, A-1180 Vienna, Austria

⁴Lorentz Institute for Theoretical Physics, Leiden University, PO Box 9506, 2300 RA Leiden, the Netherlands

Accepted XXX. Received YYY; in original form ZZZ

ABSTRACT

Recent *JWST* observations indicate that massive quiescent galaxies (stellar mass $M_* \gtrsim 10^{10} M_\odot$) at high redshift ($z \gtrsim 6$) are more abundant than predicted by most existing galaxy formation simulations and semi-analytic models. Notably, the new COLIBRE simulations have succeeded in reconciling this tension, though the precise reason for their improved agreement with *JWST* data remains unclear. We demonstrate that the improved agreement is largely due to super-Eddington growth of supermassive black holes (BHs) at high redshift. We run a series of (100 cMpc)³ simulations with the COLIBRE subgrid physics, varying the maximum allowed BH accretion rate in units of the Eddington rate. We show that only the fiducial COLIBRE model, which permits super-Eddington accretion, is consistent with the *JWST* constraints at $z \gtrsim 6$. Moreover, we find that in COLIBRE about 50 per cent of BH mass growth at high redshift occurs in the super-Eddington regime, even though such events are extremely rare in time. Our work highlights the important role of super-Eddington accretion in simulations of galaxy formation for reproducing the observed early emergence of quenching of massive galaxies.

Key words: methods: numerical – galaxies: formation – galaxies: evolution – galaxies: high-redshift

1 INTRODUCTION

Massive quiescent galaxies (MQGs) detected at high redshift ($z \gtrsim 6$) provide a powerful test for theoretical models of galaxy formation. Defined as galaxies with stellar mass $M_* \gtrsim 10^{10} M_\odot$ and negligible specific star formation rate (sSFR; e.g. $\text{sSFR} < 0.2/t_{\text{age}}(z)$ where $t_{\text{age}}(z)$ is the age of the Universe at their observed redshift), the presence of MQGs demands that realistic galaxy formation models must be able to predict their observed abundance.

The comoving number density of MQGs, n_{MQG} , is the fundamental statistic for comparing theoretical models with observations of MQGs. Unlike more traditional constraints imposed on theoretical models at low redshift, such as the observed galaxy stellar mass function (GSMF) and the size – stellar mass relation, which ensure a realistic *overall* galaxy population (see e.g. Crain et al. 2015), the abundance of MQGs at high redshift tests galaxy formation physics under *extreme* conditions. Reproducing the observed n_{MQG} at $z \gtrsim 6$ requires models to not only form massive galaxies within ≈ 1 Gyr of the Big Bang but also to quench them on an even shorter time-scale.

Before the launch of *JWST*, observations of MQGs were largely limited to $z \lesssim 4.5$ (e.g. Muzzin et al. 2013; Glazebrook et al. 2017; Schreiber et al. 2018). Those earlier data provided the first hints of a tension between theoretical galaxy formation models and observations, with the models predicting a lower n_{MQG} than observed at

high redshift (e.g. Merlin et al. 2019; Valentino et al. 2020). The first *JWST* results have exacerbated this tension, indicating that massive galaxies in the high- z Universe grew and became quiescent more rapidly than previously thought (e.g. Bunker et al. 2023; Carnall et al. 2024; Glazebrook et al. 2024; de Graaff et al. 2025a). Compared to previous instruments such as *Spitzer* and *HST*/WFC3, *JWST*’s improved infrared capabilities have enabled the detection of MQGs out to $z \approx 7.5$ (Weibel et al. 2025; Baker et al. 2025b; Yang et al. 2025), thereby putting even tighter constraints on theoretical models. The majority of existing galaxy formation simulations and semi-analytic models struggle to reproduce these new data, typically predicting n_{MQG} values that are 1 – 3 dex lower (e.g. Valentino et al. 2023; Weibel et al. 2025; Zhang et al. 2025; Baker et al. 2025a; Yang et al. 2025; Stevenson et al. 2026), though there has been recent progress in bringing some semi-analytic models closer to the data (Lagos et al. 2024).

Of particular interest is the discovery of RUBIES-UDS-QG-z7 by Weibel et al. (2025), an MQG at $z = 7.29$ identified within the RUBIES survey (de Graaff et al. 2025b) using *JWST*/NIRCam and MIRI photometry, followed up with *JWST*/NIRSpec PRISM spectroscopic observations. The authors estimated the RUBIES-UDS-QG-z7’s stellar mass $M_* \approx 10^{10.2} M_\odot$ and $\text{sSFR} < 10^{-10} \text{ yr}^{-1}$, which implies an MQG number density of $n_{\text{MQG}} \sim 10^{-6} \text{ cMpc}^{-3}$ at $z \sim 7$, providing the highest-redshift constraint on theoretical models to date. Weibel et al. (2025) showed that state-of-the-art cosmological simulations that produce realistic $z \approx 0$ galaxy populations, including

* E-mail: chaikin@strw.leidenuniv.nl

EAGLE (Schaye et al. 2015) and ILLUSTRIS-TNG (Pillepich et al. 2018), predict an insufficient abundance of MQGs to match their data.

Remarkably, the new COLIBRE simulations of galaxy formation (Schaye et al. 2025; Chaikin et al. 2025a) have been able to reconcile the discrepancies with *JWST* data on MQGs at high z (Chaikin et al. 2025b; Chandro-Gómez et al. 2025), including the tension with Weibel et al. (2025). However, the reason for this improved agreement compared to previous models remains to be fully understood. Several explanations have been proposed by Chaikin et al. (2025b), among which is super-Eddington gas accretion onto black holes (BHs).

Unlike many earlier galaxy simulations – including ILLUSTRIS (Vogelsberger et al. 2014), HORIZONAGN (Dubois et al. 2014), EAGLE, ILLUSTRIS-TNG, FABLE (Henden et al. 2018), and NewHORIZON (Dubois et al. 2021) – in COLIBRE BH accretion rates are allowed to exceed the Eddington rate, which is the rate at which radiation pressure from electron scattering balances BH gravity. Physically, this limit assumes spherical accretion, but non-spherical flows in the form of accretion-disc solutions for gas with non-zero angular momentum (e.g. Abramowicz et al. 1988; Sadowski 2009) can feature super-Eddington rates. Additionally, at sufficiently high accretion rates, photons can become trapped within the inflowing gas, reducing outward radiation pressure and allowing accretion to surpass the Eddington rate by large factors (e.g. Begelman 1979; Inayoshi et al. 2016). The presence of super-Eddington accretion is supported by observations of high- z galaxies and quasars, through inferred Eddington fractions (e.g. Farina et al. 2022; Harikane et al. 2023; Suh et al. 2025) and the necessity to grow BHs within the available cosmic time to the very high inferred BH masses (up to $\sim 10^9 M_\odot$) (e.g. Volonteri & Rees 2005; Wang et al. 2021; Farina et al. 2022; Maiolino et al. 2024; Juodžbalis et al. 2024). These results are corroborated by zoom-in hydrodynamical simulations of protoclusters (e.g. Lupi et al. 2024; Bennett et al. 2024; Huško et al. 2025b) and by semi-analytic models (e.g. Pezzulli et al. 2016; Trinca et al. 2024).

Furthermore, those earlier simulations of galaxy formation were typically run in relatively small volumes ($\sim 100^3 \text{ cMpc}^3$), limiting the minimum non-zero n_{MQG} they could predict to $\sim 10^{-6} \text{ cMpc}^{-3}$ and making their predicted n_{MQG} prone to cosmic variance (e.g. Thomas et al. 2023), which could exacerbate the tension with *JWST* data found in earlier comparisons. Indeed, Lovell et al. (2023) used the FLARES simulations (Lovell et al. 2021) – zoom-in simulations with a parent volume of $(3.2 \text{ cGpc})^3$ using the original EAGLE model – to extend the predictions of the EAGLE simulations for non-zero n_{MQG} from $z \approx 5$ up to $z \approx 8$. Turner et al. (2025) performed mock observations of FLARES galaxies, finding that this larger volume does not resolve the tension with Weibel et al. (2025). They concluded that, while accounting for systematic uncertainties in the data may alleviate the tension, achieving full agreement likely requires modifications to the modelling of BHs and AGN feedback in EAGLE, such as allowing for super-Eddington accretion.

In this work, we investigate the importance of super-Eddington BH growth for resolving the tension between theoretical predictions and the observed $z \gtrsim 6$ abundance of MQGs. We do so by comparing predictions from the new COLIBRE simulations of galaxy formation¹ (Schaye et al. 2025; Chaikin et al. 2025a), using models with different maximum allowed BH accretion rates. Section 2 describes our methodology, Section 3 presents the results, and Section 4 summarizes our conclusions.

2 METHODS

2.1 The COLIBRE simulations

The COLIBRE simulations are described extensively in Schaye et al. (2025). Below, we only provide a summary.

The COLIBRE simulations were run using the astrophysical code SWIFT (Schaller et al. 2024), with gas hydrodynamics solved using the smoothed particle hydrodynamics (SPH) scheme SPHENIX (Borrow et al. 2022). The initial conditions were generated at $z = 63$ by the MONOFONIC code (Hahn et al. 2020; Michaux et al. 2021) using second-order Lagrangian perturbation theory. The assumed cosmology is the Λ CDM ‘3x2pt + all external constraints’ cosmology (Abbott et al. 2022): $\Omega_{\text{m},0} = 0.306$, $\Omega_{\text{b},0} = 0.0486$, $\sigma_8 = 0.807$, $h = 0.681$, $n_s = 0.967$, with a single massive neutrino species of 0.06 eV. The COLIBRE simulations include three resolutions: m7 (gas and dark matter (DM) particle masses of $m_{\text{gas}} = 1.47 \times 10^7 M_\odot$ and $m_{\text{dm}} = 1.94 \times 10^7 M_\odot$, respectively), m6 ($m_{\text{gas}} = 1.8 \times 10^6 M_\odot$, $m_{\text{dm}} = 2.4 \times 10^6 M_\odot$), and m5 ($m_{\text{gas}} = 2.3 \times 10^5 M_\odot$, $m_{\text{dm}} = 3.0 \times 10^5 M_\odot$), with simulations at lower resolutions available in larger volumes (up to 400^3 cMpc^3 for m7; see table 2 in Schaye et al. 2025). At m7 resolution, the Plummer-equivalent gravitational softening length for baryons and DM is set to the minimum of 1.4 proper kpc (pkpc) and 3.6 comoving kpc, while at m6 (m5) resolution, it is reduced by a factor of 2 (4) relative to m7.

The radiative cooling and heating rates for primordial elements and their free electrons are calculated using the non-equilibrium thermochemistry solver CHIMES (Richings et al. 2014a,b). The rates for metals are provided by HYBRID-CHIMES (Ploeckinger et al. 2025), which uses tabulated species fractions computed by CHIMES assuming ionization equilibrium and steady-state chemistry, corrected for the non-equilibrium electron density from hydrogen and helium. The gas chemical composition is tracked by modelling the abundances of 12 individual elements, which are diffused among SPH gas neighbours using a velocity shear-based model for turbulent mixing (Correa et al., submitted). COLIBRE models the formation and evolution of dust grains (Trayford et al. 2025), which are coupled to the CHIMES solver.

Star-forming gas particles are identified using a gravitational instability criterion, following Nobels et al. (2024). The Schmidt (1959) law, with a star formation efficiency per free-fall time $\varepsilon = 0.01$, is used to compute SFRs of star-forming particles, which are stochastically converted into stars. Newly formed stellar particles represent simple stellar populations with a Chabrier (2003) initial stellar mass function, injecting energy, momentum, and metals into their nearby gas. Feedback from core-collapse SNe is modelled following Dalla Vecchia & Schaye (2012); Chaikin et al. (2023), with modifications as described in Schaye et al. (2025). COLIBRE also includes SN type-Ia feedback and three early stellar feedback processes: H II regions, stellar winds, and radiation pressure (Benítez-Llambay et al. 2025).

BHs are represented by collisionless BH particles. BH particles are seeded by converting the densest gas particle in a Friends-of-Friends (FoF) halo into a BH particle. At m7 resolution, seeding occurs when the halo FoF mass exceeds a threshold of $5 \times 10^{10} M_\odot$, provided the FoF halo does not already contain a BH. BH particles grow in mass by accreting surrounding gas and by merging with other BHs. The accretion rate onto BHs is computed using the modified Bondi-Hoyle-Lyttleton formula (Bondi 1952; Hoyle & Lyttleton 1939), with turbulence and vorticity corrections from Krumholz et al. (2006), and is capped at 100 times the Eddington rate² (i.e. permitting super-

¹ <https://colibre-simulations.org>

² The choice to allow super-Eddington BH accretion in COLIBRE is motivated

Eddington accretion). Dynamical friction and BH-BH mergers are modelled following [Bahé et al. \(2022\)](#).

At each resolution, the **COLIBRE** simulations include models with purely thermal AGN feedback and hybrid AGN feedback (which combines bipolar kinetic jets with thermal energy injections and accounts for the evolution of BH spin; [Huško et al. 2025a](#)). Thermal AGN feedback is implemented deterministically, following [Booth & Schaye \(2009\)](#), but with a modification: BH particles heat their neighbouring gas by a temperature increment proportional to the BH (subgrid) mass, $\Delta T_{\text{AGN}} \propto m_{\text{BH}}$, rather than by a fixed ΔT_{AGN} (see [Schaye et al. 2025](#), for details). This work uses only the simulations with purely thermal AGN feedback, which is the fiducial AGN feedback model in **COLIBRE**. In the thermal model, the radiative efficiency of the subgrid accretion disc is assumed to be 10 per cent, and the BH seed mass at m7 resolution is $10^{5.5} \text{ M}_\odot$. The strengths of the **COLIBRE** SN and AGN energy feedback were optimised to reproduce the observed $z = 0$ GSMF from GAMA DR4 ([Driver et al. 2022](#)), the observed $z \approx 0$ galaxy stellar mass – size relation reported by [Hardwick et al. \(2022\)](#), and the $z \approx 0$ masses of BHs in massive galaxies, as detailed in [Chaikin et al. \(2025a\)](#) for the thermal AGN feedback and in [Huško et al. \(2025a\)](#) for the hybrid feedback simulations.

The **COLIBRE** simulations produce 128 data outputs between $z = 30$ and 0 (see [Schaye et al. 2025](#), for details). Subhaloes are identified using the history-based halo finder HBT-HERONS ([Han et al. 2018](#); [Forouhar Moreno et al. 2025](#)). The HBT-HERONS output is processed with the Spherical Overdensity and Aperture Processor (SOAP; [McGibbon et al. 2025](#)) to generate a comprehensive catalogue of halo and galaxy properties. From SOAP, we use galaxy stellar mass M_* and star formation rate (SFR), computed by summing the masses of stellar particles and the instantaneous SFRs of gas particles, respectively. These particles must be gravitationally bound to the subhalo and located within a 3D spherical aperture of radius 50 pkpc, which is the default choice in **COLIBRE**. For the M_* – BH mass relation, we take the (subgrid) mass of the BH particle that is bound to the subhalo and within 50 pkpc. If a subhalo contains more than one such BH, the mass of the most massive BH is used; if no BH is bound, the BH mass assigned to that subhalo is zero. Finally, all properties intrinsic to BH particles, such as the instantaneous Eddington fraction and the cumulative energy injected by AGN feedback, are taken directly from the snapshot output.

2.2 Model variations

In **COLIBRE**, the BH accretion rate, \dot{m}_{BH} , is capped at 100 times the Eddington rate, \dot{m}_{Edd} (i.e. the Eddington fraction $f_{\text{Edd}} \equiv \dot{m}_{\text{BH}}/\dot{m}_{\text{Edd}}$ cannot exceed $f_{\text{Edd,max}} = 10^2$). To demonstrate the importance of super-Eddington accretion, we ran two new simulations where (i) we capped the accretion rate at the Eddington limit ($f_{\text{Edd,max}} = 1$) and (ii) at 10 per cent thereof ($f_{\text{Edd,max}} = 0.1$). These two models were run in a 100^3 cMpc^3 volume at m7 resolution, with all other parameters matching the fiducial **COLIBRE** m7 model with thermal AGN feedback, for which $f_{\text{Edd,max}} = 10^2$. We chose this volume and resolution as it was our only computationally feasible option that could produce realistic non-zero number densities of MQGs at high z ($\sim 10^{-6} \text{ cMpc}^{-3}$). For consistency with the variation simulations, we use the fiducial simulation with the same volume and resolution³,

by the growing observational evidence (see Section 1), while the cap of 10^2 (which is hardly ever reached in practice) is imposed for numerical reasons.

³ More precisely, instead of using the L100m7 simulation from the original **COLIBRE** suite, we re-ran this simulation with extra BH-related output, which

although the fiducial model is also available in $8\times$ and $64\times$ larger volumes (see table 2 in [Schaye et al. 2025](#)).

3 RESULTS

Fig. 1 shows the evolution of several properties of a representative massive galaxy and its central BH from $z = 12$ to 4. Each panel shows three solid curves, corresponding to our fiducial model with $f_{\text{Edd,max}} = 10^2$ and its variations with $f_{\text{Edd,max}} = 1$ and 0.1. The same galaxy, cross-matched across the three L100m7 simulations, which use identical initial conditions, is shown in all cases. The galaxy resides in a central halo whose total mass grows from $M_{200c} \sim 10^{10} \text{ M}_\odot$ at $z = 12$ to $\sim 10^{12.5} \text{ M}_\odot$ by $z = 4$. The top left panel shows the galaxy stellar mass M_* , the top middle panel its instantaneous sSFR ($\equiv \text{SFR}/M_*$), and the top right panel the mass of its BH. In addition, the three long-dashed curves in the top right panel indicate the accreted BH mass in the simulations (i.e. excluding the seed mass and mass gained via mergers), while the two black dotted lines show the theoretical BH mass evolution for continuous accretion at $f_{\text{Edd}} = 0.1$ and 1 (without mergers), starting at $z = 10$ and $z = 9$, respectively.

In the three simulations, the galaxy and its BH evolve nearly identically from $z = 12$ until $z \approx 9$, with minor differences resulting from stochastic effects (e.g. [Borrow et al. 2023](#)). Below $z \approx 9$, the solid curves in the top right panel start to diverge as the BHs begin to grow rapidly via gas accretion, with the models with lower $f_{\text{Edd,max}}$ predicting slower BH growth. Comparison of the yellow, red, and blue curves to the black dotted lines between $z \approx 7$ and 9 confirms that the BH in the fiducial model undergoes super-Eddington growth, while the growth in the $f_{\text{Edd,max}} = 1$ and $f_{\text{Edd,max}} = 0.1$ models proceeds at ≈ 100 and 10 per cent of the Eddington rate. The faster BH growth triggers an earlier onset of AGN feedback. Consequently, the galaxy in the $f_{\text{Edd,max}} = 10^2$ simulation becomes quiescent below $z \approx 7$. In contrast, with $f_{\text{Edd,max}} = 1$, the same galaxy continues actively forming stars until $z \approx 6$, while with $f_{\text{Edd,max}} = 0.1$, it remains star-forming throughout the entire redshift range explored.

The bottom row of Fig. 1 provides further insight into the properties of the BH: the instantaneous Eddington fraction f_{Edd} (left); the cumulative AGN feedback energy injected into the nearby gas (middle); and the cumulative fraction of mass accreted in the super-Eddington regime (right), which is defined for each redshift as the mass accreted at $f_{\text{Edd}} > 1$ up to that redshift, $m_{\text{acc},f_{\text{Edd}}>1}$, divided by the total accreted mass, $m_{\text{acc},\text{total}}$. The yellow squares in the left panel mark individual super-Eddington accretion events (i.e. time-steps with $f_{\text{Edd}} > 1$) experienced by the BH in the fiducial simulation, which have a much higher cadence than the standard **COLIBRE** output. The BH in the fiducial model experiences numerous super-Eddington accretion events between $z = 9$ and 7, with the highest rate exceeding the Eddington limit by a factor ~ 10 . In the two variation models, f_{Edd} hits a ceiling at the corresponding $f_{\text{Edd,max}}$ value around $z \approx 9$ and follows it until $z \approx 6$ ($z = 4$) for $f_{\text{Edd,max}} = 1$ ($f_{\text{Edd,max}} = 0.1$).

Once the BH has injected enough AGN energy to quench the star formation in its host galaxy, f_{Edd} drops to $\sim 10^{-3} - 10^{-1}$, which occurs below $z \approx 7$ and $z \approx 6$ in the $f_{\text{Edd,max}} = 10^2$ and $f_{\text{Edd,max}} = 1$ models, respectively. After this point, the rapid gas accretion phase halts, and the BH subsequently grows slowly in a self-regulated regime. Although, for this particular galaxy, the $f_{\text{Edd,max}} = 1$ model predicts an initially slower BH growth compared to $f_{\text{Edd,max}} = 10^2$, the earlier

we needed in this work. We verified that the results from the two simulations are statistically indistinguishable.

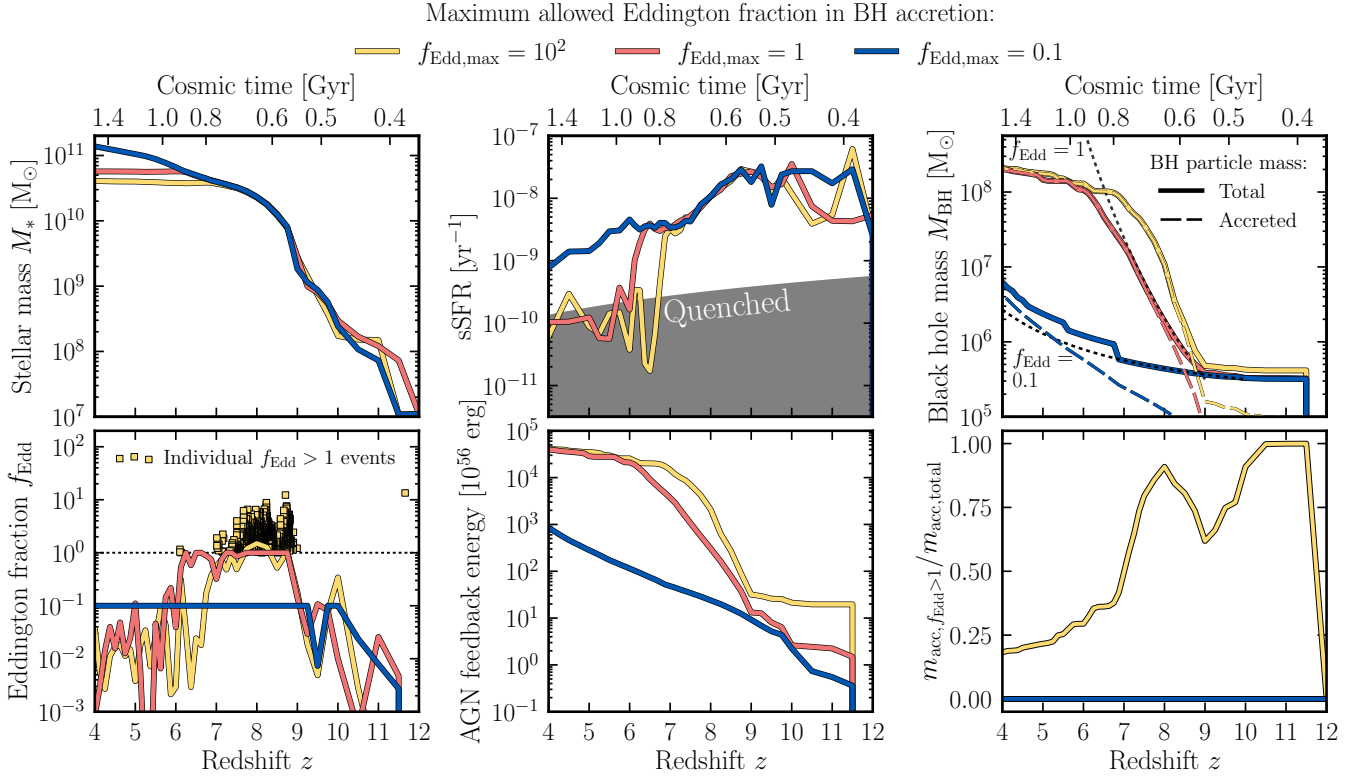


Figure 1. An example of a representative massive galaxy whose star formation is quenched by AGN feedback in the simulations with different maximum allowed Eddington fractions: $f_{\text{Edd},\text{max}} = 10^2$ (yellow), 1 (red), and 0.1 (blue). In all three cases, the evolution of the same galaxy is shown. From left to right, the top row shows the galaxy stellar mass, its sSFR, and its BH mass. The bottom row shows the Eddington fraction, the cumulative AGN feedback energy injected by the BH, and the cumulative fraction of mass accreted by the BH in $f_{\text{Edd}} > 1$ accretion events (see the main text for details). Allowing super-Eddington accretion results in enhanced BH growth at high redshift, leading to the galaxy becoming quenched by AGN feedback at earlier times.

quenching for $f_{\text{Edd},\text{max}} = 10^2$ allows the BH in the $f_{\text{Edd},\text{max}} = 1$ model to catch up in mass, resulting in nearly identical final BH masses at $z \lesssim 6$. Finally, the bottom right panel shows that, at the time when the BH quenches its host galaxy in the $f_{\text{Edd},\text{max}} = 10^2$ model, about 50 per cent of its accreted mass was accreted at super-Eddington rates.

Having illustrated the main differences between models with different $f_{\text{Edd},\text{max}}$ for a single massive galaxy, we next examine the evolution of all massive galaxies in the simulated volumes. Fig. 2 shows the redshift evolution from $z = 7.5$ to 6 of the sSFR – M_* relation (top row); the BH mass – M_* relation (middle row); and the cumulative fraction of BH mass accreted at $f_{\text{Edd}} > 1$, $m_{\text{acc},f_{\text{Edd}}>1}/m_{\text{acc},\text{total}}$, versus M_* (bottom row). At $z = 7.5$, the sSFR – M_* relation is indistinguishable between the three models, with all galaxies following the star-forming main sequence (SFMS). Clear differences emerge, however, in the BH mass – M_* relation: the masses of BHs in massive galaxies ($M_* \gtrsim 10^{10} M_\odot$) are $\approx 0.5\text{--}0.7$ dex higher for $f_{\text{Edd},\text{max}} = 10^2$ than for $f_{\text{Edd},\text{max}} = 1$, while in the $f_{\text{Edd},\text{max}} = 0.1$ model, all BHs remain close to their seed mass of $10^{5.5} M_\odot$. At $z = 7$, the $f_{\text{Edd},\text{max}} = 10^2$ model produces its first MQG (yellow circle), while galaxies in the other two models remain on the SFMS. By $z = 6.5$, the fiducial model predicts three MQGs, whereas the others continue to follow the SFMS. Only at $z = 6$ does the $f_{\text{Edd},\text{max}} = 1$ model produce its first MQGs, with a number a factor of three lower than in the fiducial model. In both models, the BH masses in most MQGs are higher than the median BH mass – M_* relation, indicating the dominant role of AGN feedback in driving the quenching.

Fig. 3 compares the predicted number density of MQGs in the simulations, n_{MQG} , with recent *JWST* constraints at $z > 6$. We

include data from [Baker et al. \(2025b\)](#) and [Russell et al. \(2025\)](#), who define MQGs as $M_* > 10^{9.5} M_\odot$ and $\text{sSFR} < 0.2/t_{\text{age}}$; from [Yang et al. \(2025\)](#), corresponding to $10^{9.5} < M_*/M_\odot < 10^{10.6}$ and $\text{sSFR} < 0.2/t_{\text{age}}$; and a single galaxy-based estimate from [Weibel et al. \(2025\)](#), with $M_* \approx 10^{10.2} M_\odot$ and $\text{sSFR} < 10^{-10} \text{ yr}^{-1}$. To maximize consistency with these selection criteria, we define MQGs in the simulations as galaxies with $M_* > 10^{9.5} M_\odot$ and $\text{sSFR} < 0.2/t_{\text{age}}$. To ensure a consistent comparison with [Yang et al. \(2025\)](#) whose selection excludes galaxies with $M_* > 10^{10.6} M_\odot$, we show their data only at $z > 6.5$, where our and their criteria effectively align because at $z > 6.5$ all simulated MQGs have stellar masses $10^{10} < M_*/M_\odot < 10^{10.6}$ (see Fig. 2). To account for measurement uncertainties present in observations, we add errors to simulated SFRs and M_* sampled from a lognormal distribution with zero mean and a standard deviation of 0.3 dex (e.g. [Zhang et al. 2025](#)). We repeat this process 300 times, yielding a distribution of n_{MQG} values in each redshift bin. We then plot the median values (solid curves), the maximum of the 16th–84th percentile range and Poisson uncertainties (shaded regions), and the predictions without measurement uncertainties (dotted curves). We note that the added uncertainties have a significant effect on n_{MQG} only for the $f_{\text{Edd},\text{max}} = 0.1$ model.

Only the fiducial model, which allows super-Eddington accretion, is consistent with the *JWST* data at $z > 6$, in line with the earlier results from the *COLIBRE* simulations in larger volumes ([Chaikin et al. 2025b](#); [Chandro-Gómez et al. 2025](#)). In contrast, the $f_{\text{Edd},\text{max}} = 1$ model predicts no MQGs at $z > 6.25$, while $f_{\text{Edd},\text{max}} = 0.1$ struggles to produce even a single MQG (none are present if no measurement errors are included). The $f_{\text{Edd},\text{max}} = 10^2$ and $f_{\text{Edd},\text{max}} = 1$ models

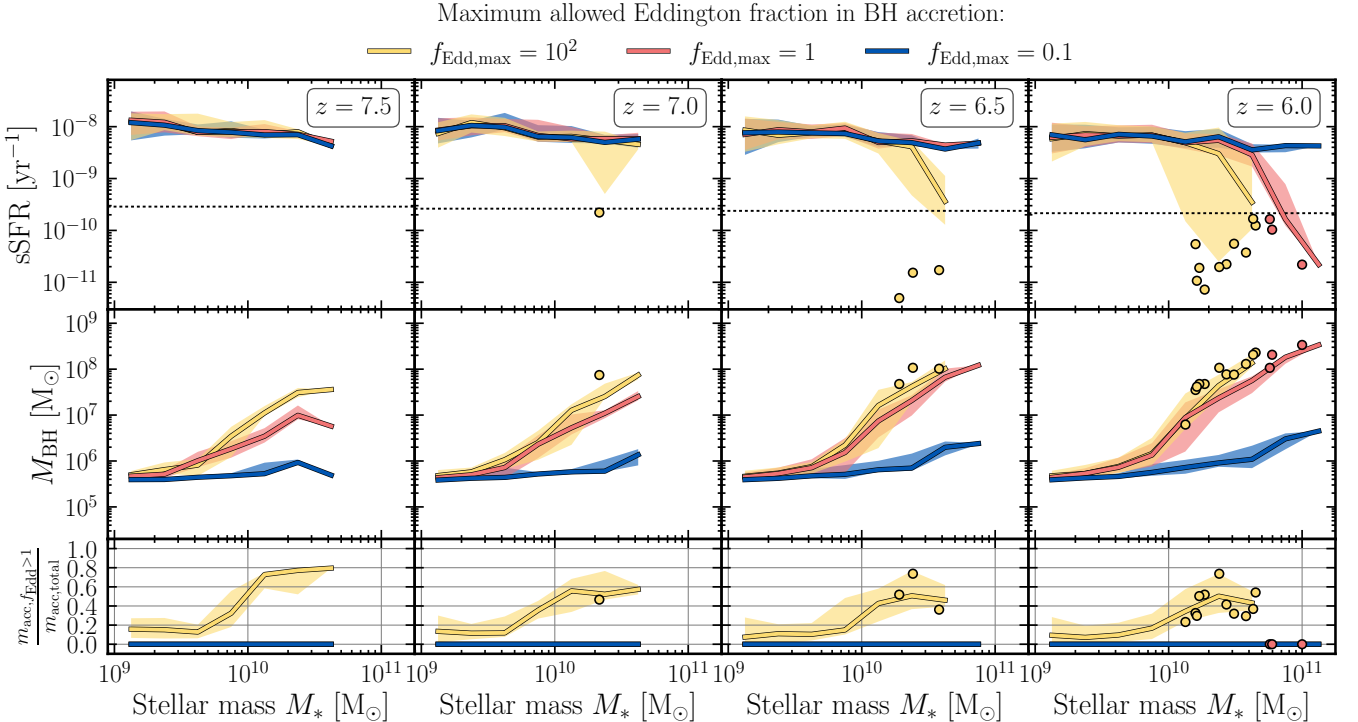


Figure 2. Evolution of the sSFR (top), BH mass (middle), and the cumulative fraction of BH mass accreted at $f_{\text{Edd}} > 1$, all plotted against stellar mass. Results are shown for simulations with $f_{\text{Edd},\text{max}} = 10^2$, 1, and 0.1 (colours). Columns show different redshifts (left to right): 7.5, 7, 6.5, and 6. Solid lines indicate the median relations and shaded regions the 16th to 84th percentiles, all computed in 0.2-dex M_* bins. In the top panels, the black horizontal lines mark the quenching threshold of $0.2/t_{\text{age}}$. Individual circles denote all MQGs satisfying $\text{sSFR} < 0.2/t_{\text{age}}$ and $M_* > 10^{9.5} M_\odot$. The enhanced BH growth due to super-Eddington accretion is evident across the entire population of massive galaxies, enabling their earlier quenching by AGN feedback and leading to a larger number of MQGs.

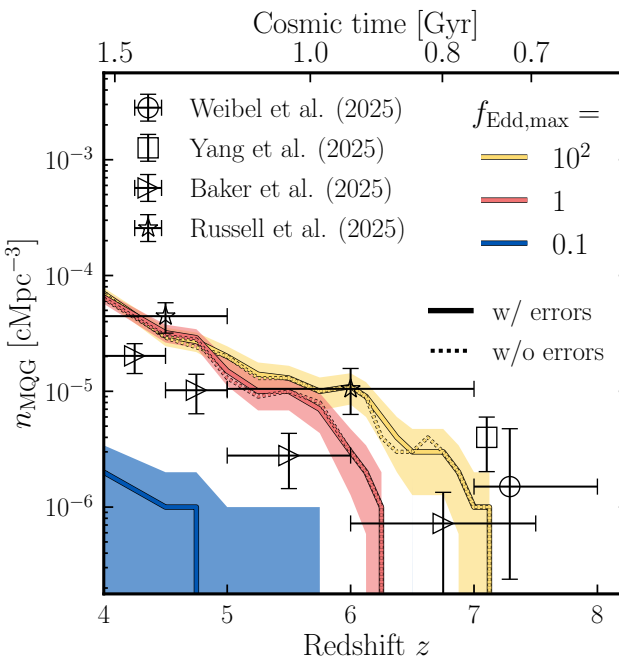


Figure 3. Evolution of the comoving number density of MQGs in simulations with different maximum allowed Eddington fractions: $f_{\text{Edd},\text{max}} = 10^2$ (yellow), 1 (red), and 0.1 (blue). Solid curves show predictions after adding 0.3 dex lognormal errors to SFRs and M_* ; dotted curves show results without errors. Black symbols indicate JWST constraints. Only the fiducial model ($f_{\text{Edd},\text{max}} = 10^2$), which allows super-Eddington BH accretion, is consistent with the JWST data at $z \gtrsim 6$.

converge below $z \approx 5$, as BHs in the $f_{\text{Edd},\text{max}} = 1$ model eventually catch up in mass (and therefore in the energy injected by AGN feedback) with those in the fiducial model (as shown in Fig. 1). At $z < 5$, the converged models are consistent with Russell et al. (2025) but lie ≈ 0.5 dex above Baker et al. (2025b) (see Chaikin et al. 2025b; Chandro-Gómez et al. 2025, for details). At $z = 0$, the GSMF, galaxy size – M_* relation, and BH mass – M_* relation – the three relations used to calibrate SN and AGN feedback in COLIBRE – are statistically indistinguishable between the $f_{\text{Edd},\text{max}} = 10^2$ and $f_{\text{Edd},\text{max}} = 1$ models (not shown).

Finally, the top (bottom) panel of Fig. 4 shows the cumulative fraction of BH mass accreted (time spent) in accretion events with different Eddington fractions for the fiducial model. The numerator and denominator of the cumulative fractions are computed as sums over all BH particles in the simulation. The fraction of time spent by BHs accreting at $f_{\text{Edd}} > 1$ is at most a few per cent at high redshift and decreases to negligible values by $z = 0$, even though these super-Eddington events account for a significant fraction of BH mass growth (50 – 70 per cent at $z \gtrsim 7$, as can be seen in this figure and Figs. 1 and 2). In other words, this figure shows that although super-Eddington accretion is not sustained over long time-scales, it is responsible for substantial BH growth.

4 CONCLUSIONS

We have investigated the importance of super-Eddington BH growth for alleviating the tension between galaxy formation models and $z \gtrsim 6$ JWST constraints on the abundance of MQGs. Using the COLIBRE galaxy formation model (Schaye et al. 2025; Chaikin et al.

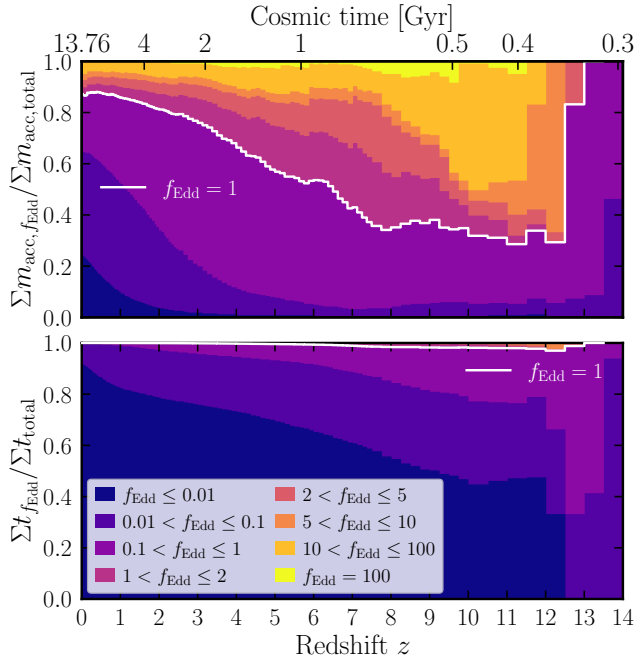


Figure 4. Cumulative fraction of BH mass accreted (top panel) and time spent (bottom panel) in accretion events at different Eddington fractions (colour-coded). Results are shown for the model with $f_{\text{Edd},\text{max}} = 10^2$, using all BH particles in the simulation to calculate the cumulative fractions. The white curve marks $f_{\text{Edd}} = 1$ for reference. Although super-Eddington accretion ($f_{\text{Edd}} > 1$) contributes more than ≈ 50 per cent of the BH mass growth at high redshift, with $f_{\text{Edd}} \gtrsim 10$ frequently reached, BHs spend only a few per cent of their time in the super-Eddington regime.

2025a), we ran two simulations in a $(100 \text{ cMpc})^3$ volume with BH accretion rates capped at Eddington fraction of $f_{\text{Edd},\text{max}} = 1$ and 0.1 , complementing the fiducial model where the cap is $f_{\text{Edd},\text{max}} = 10^2$ (i.e. allowing super-Eddington accretion). Our main findings are as follows:

- Super-Eddington accretion is readily realized in the fiducial COLIBRE model during the rapid phase of gas accretion onto BHs at high redshift, with Eddington fractions of $f_{\text{Edd}} \sim 10$ frequently reached (Fig. 1). This significantly enhances BH mass growth, leading to an earlier onset of AGN feedback and, consequently, to earlier quenching of the massive galaxies hosting the BHs.
- The enhanced BH growth at high redshift due to super-Eddington accretion is evident across the entire population of massive galaxies (Fig. 2). By $z = 6$, as much as ≈ 50 per cent of the accreted mass of BHs in massive galaxies has been accreted at super-Eddington rates, even though BHs spend only a few per cent of their time accreting at $f_{\text{Edd}} > 1$ (Fig. 4).
- The enhanced BH growth renders the fiducial COLIBRE model consistent with *JWST* constraints on the number density of MQGs at $z \gtrsim 6$, whereas the $f_{\text{Edd},\text{max}} = 1$ and $f_{\text{Edd},\text{max}} = 0.1$ models strongly undershoot the high-redshift data (Fig. 3).

Taken together, the results of our cosmological simulations provide strong evidence that super-Eddington accretion offers a promising solution to the tension between predictions from galaxy formation simulations adopting the ΛCDM cosmology and the high-redshift number densities of MQGs revealed by *JWST*.

In closing, we emphasize that the COLIBRE simulations reproduce the observed evolution of the GSMF at $0 < z < 12$ (Chaikin et al. 2025b) and are consistent with the sizes and star formation histories

of observed MQGs at high redshift (Chandro-Gómez et al. 2025). This agreement suggests that, although BH physics in COLIBRE is necessarily captured rather crudely given the limited simulation resolution, the effective impact of AGN feedback on resolved galactic scales is not unrealistic. The analysis in this work is subject to cosmic variance, as the simulated volume is relatively small (100^3 cMpc^3). However, Chaikin et al. (2025b) show that the fiducial COLIBRE model remains consistent with the $z > 6$ *JWST* data in $8\times$ and $64\times$ larger volumes, as well as at higher resolution. Finally, we note that in COLIBRE, super-Eddington accretion is not limited to m7 resolution, but is also an important mechanism for BH growth at the higher m6 and m5 resolutions.

ACKNOWLEDGEMENTS

This work used the DiRAC@Durham facility managed by the Institute for Computational Cosmology on behalf of the STFC DiRAC HPC Facility (www.dirac.ac.uk). The equipment was funded by BEIS capital funding via STFC capital grants ST/K00042X/1, ST/P002293/1, ST/R002371/1 and ST/S002502/1, Durham University and STFC operations grant ST/R000832/1. DiRAC is part of the National e-Infrastructure. This project has received funding from the Netherlands Organization for Scientific Research (NWO) through research programme Athena 184.034.002. CGL acknowledges support from STFC consolidated grant ST/X001075/1. SP acknowledges support by the Austrian Science Fund (FWF) through grant-DOI: 10.55776/V982. The research in this paper made use of the SWIFT open-source simulation code (<http://www.swiftsim.com>, Schaller et al. 2024) version 1.0.0.

DATA AVAILABILITY

The data underlying this article will be shared on reasonable request to the corresponding author. The public version of the SWIFT simulation code can be found on www.swiftsim.com. The SWIFT modules related to the COLIBRE galaxy formation model will be integrated into the public version after the public release of COLIBRE. The CHIMES astrochemistry code is publicly available at <https://richings.bitbucket.io/chimes/home.html>. The HBT-HERONS halo finder is available at <https://hbt-herons.strw.leidenuniv.nl/>.

REFERENCES

Abbott T. M. C., et al., 2022, *Phys. Rev. D*, **105**, 023520
 Abramowicz M. A., Czerny B., Lasota J. P., Szuszkiewicz E., 1988, *ApJ*, **332**, 646
 Bahé Y. M., et al., 2022, *MNRAS*, **516**, 167
 Baker W. M., et al., 2025a, *MNRAS*, **539**, 557
 Baker W. M., et al., 2025b, *A&A*, **702**, A270
 Begelman M. C., 1979, *MNRAS*, **187**, 237
 Benítez-Llambay A., et al., 2025, *arXiv e-prints*, p. arXiv:2509.25309
 Bennett J. S., Sijacki D., Costa T., Laporte N., Witten C., 2024, *MNRAS*, **527**, 1033
 Bondi H., 1952, *MNRAS*, **112**, 195
 Booth C. M., Schaye J., 2009, *MNRAS*, **398**, 53
 Borrow J., Schaller M., Bower R. G., Schaye J., 2022, *MNRAS*, **511**, 2367
 Borrow J., Schaller M., Bahé Y. M., Schaye J., Ludlow A. D., Ploeckinger S., Nobels F. S. J., Altamura E., 2023, *MNRAS*, **526**, 2441
 Bunker A. J., et al., 2023, *A&A*, **677**, A88
 Carnall A. C., et al., 2024, *MNRAS*, **534**, 325

Chabrier G., 2003, *PASP*, **115**, 763

Chaikin E., Schaye J., Schaller M., Benítez-Llambay A., Nobels F. S. J., Ploeckinger S., 2023, *MNRAS*, **523**, 3709

Chaikin E., et al., 2025a, arXiv e-prints, p. arXiv:2509.04067

Chaikin E., et al., 2025b, arXiv e-prints, p. arXiv:2509.07960

Chandro-Gómez Á., et al., 2025, arXiv e-prints, p. arXiv:2512.16208

Crain R. A., et al., 2015, *MNRAS*, **450**, 1937

Dalla Vecchia C., Schaye J., 2012, *MNRAS*, **426**, 140

Driver S. P., et al., 2022, *MNRAS*, **513**, 439

Dubois Y., et al., 2014, *MNRAS*, **444**, 1453

Dubois Y., et al., 2021, *A&A*, **651**, A109

Farina E. P., et al., 2022, *ApJ*, **941**, 106

Forouhar Moreno V. J., Helly J., McGibbon R., Schaye J., Schaller M., Han J., Kugel R., Bahé Y. M., 2025, *MNRAS*, **543**, 1339

Glazebrook K., et al., 2017, *Nature*, **544**, 71

Glazebrook K., et al., 2024, *Nature*, **628**, 277

de Graaff A., et al., 2025a, *Nature Astronomy*, **9**, 280

de Graaff A., et al., 2025b, *A&A*, **697**, A189

Hahn O., Michaux M., Rampf C., Uhlemann C., Angulo R. E., 2020, MUSIC2-monofonIC: 3LPT initial condition generator, Astrophysics Source Code Library, record ascl:2008.024 (ascl:2008.024)

Han J., Cole S., Frenk C. S., Benitez-Llambay A., Helly J., 2018, *MNRAS*, **474**, 604

Hardwick J. A., Cortese L., Obreschkow D., Catinella B., Cook R. H. W., 2022, *MNRAS*, **509**, 3751

Harikane Y., et al., 2023, *ApJ*, **959**, 39

Henden N. A., Puchwein E., Shen S., Sijacki D., 2018, *MNRAS*, **479**, 5385

Hoyle F., Lyttleton R. A., 1939, *Proceedings of the Cambridge Philosophical Society*, **35**, 405

Huško F., et al., 2025a, arXiv e-prints, p. arXiv:2509.05179

Huško F., Lacey C. G., Roper W. J., Schaye J., Briggs J. M., Schaller M., 2025b, *MNRAS*, **537**, 2559

Inayoshi K., Haiman Z., Ostriker J. P., 2016, *MNRAS*, **459**, 3738

Juodžbalis I., et al., 2024, *Nature*, **636**, 594

Krumholz M. R., McKee C. F., Klein R. I., 2006, *ApJ*, **638**, 369

Lagos C. d. P., et al., 2024, *MNRAS*, **531**, 3551

Lovell C. C., Vijayan A. P., Thomas P. A., Wilkins S. M., Barnes D. J., Irodou D., Roper W., 2021, *MNRAS*, **500**, 2127

Lovell C. C., et al., 2023, *MNRAS*, **525**, 5520

Lupi A., Quadri G., Volonteri M., Colpi M., Regan J. A., 2024, *A&A*, **686**, A256

Maiolino R., et al., 2024, *A&A*, **691**, A145

McGibbon R., Helly J., Schaye J., Schaller M., Vandenbroucke B., 2025, *The Journal of Open Source Software*, **10**, 8252

Merlin E., et al., 2019, *MNRAS*, **490**, 3309

Michaux M., Hahn O., Rampf C., Angulo R. E., 2021, *MNRAS*, **500**, 663

Muzzin A., et al., 2013, *ApJ*, **777**, 18

Nobels F. S. J., Schaye J., Schaller M., Ploeckinger S., Chaikin E., Richings A. J., 2024, *MNRAS*, **532**, 3299

Pezzulli E., Valiante R., Schneider R., 2016, *MNRAS*, **458**, 3047

Pillepich A., et al., 2018, *MNRAS*, **473**, 4077

Ploeckinger S., Richings A. J., Schaye J., Trayford J. W., Schaller M., Chaikin E., 2025, arXiv e-prints, p. arXiv:2506.15773

Richings A. J., Schaye J., Oppenheimer B. D., 2014a, *MNRAS*, **440**, 3349

Richings A. J., Schaye J., Oppenheimer B. D., 2014b, *MNRAS*, **442**, 2780

Russell T. A., et al., 2025, *MNRAS*, **544**, 4482

Schaller M., et al., 2024, *MNRAS*, **530**, 2378

Schaye J., et al., 2015, *MNRAS*, **446**, 521

Schaye J., et al., 2025, arXiv e-prints, p. arXiv:2508.21126

Schmidt M., 1959, *ApJ*, **129**, 243

Schreiber C., et al., 2018, *A&A*, **618**, A85

Sądowski A., 2009, *ApJS*, **183**, 171

Stevenson S. D., et al., 2026, *MNRAS*, **545**, staf2087

Suh H., et al., 2025, *Nature Astronomy*, **9**, 271

Thomas P. A., Lovell C. C., Maltz M. G. A., Vijayan A. P., Wilkins S. M., Irodou D., Roper W. J., Seeyave L., 2023, *MNRAS*, **524**, 43

Trayford J. W., et al., 2025, arXiv e-prints, p. arXiv:2505.13056

Trinca A., et al., 2024, arXiv e-prints, p. arXiv:2412.14248

This paper has been typeset from a \TeX / \LaTeX file prepared by the author.